The extent and strength of electrical coupling between inferior olivary neurons is heterogeneous

Gregory J. Hoge, Kimberly G. V. Davidson, Thomas Yasumura, Pablo E. Castillo, John E. Rash and Alberto E. Pereda

J Neurophysiol 105:1089-1101, 2011. First published 22 December 2010; doi:10.1152/jn.00789.2010

J Neurophysiol 105: 1089–1101, 2011.
First published December 22, 2010; doi:10.1152/jn.00789.2010.

The extent and strength of electrical coupling between inferior olivary neurons is heterogeneous

Gregory J. Hoge,[1] Kimberly G. V. Davidson,[2] Thomas Yasumura,[2] Pablo E. Castillo,[1] John E. Rash,[2] and Alberto E. Pereda[1]

[1]*Dominick P. Purpura Department of Neuroscience, Albert Einstein College of Medicine, Bronx, New York; and* [2]*Department of Biomedical Sciences, Colorado State University, Fort Collins, Colorado*

Submitted 14 September 2010; accepted in final form 16 December 2010

Hoge GJ, Davidson KG, Yasumura T, Castillo PE, Rash JE, Pereda AE. The extent and strength of electrical coupling between inferior olivary neurons is heterogeneous. *J Neurophysiol* 105: 1089–1101, 2011. First published December 22, 2010; doi:10.1152/jn.00789.2010.—Gap junctions constitute the only form of synaptic communication between neurons in the inferior olive (IO), which gives rise to the climbing fibers innervating the cerebellar cortex. Although its exact functional role remains undetermined, electrical coupling was shown to be necessary for the transient formation of functional compartments of IO neurons and to underlie the precise timing of climbing fibers required for cerebellar learning. So far, most functional considerations assume the existence of a network of permanently and homogeneously coupled IO neurons. Contrasting this notion, our results indicate that coupling within the IO is highly variable. By combining tracer-coupling analysis and paired electrophysiological recordings, we found that individual IO neurons could be coupled to a highly variable number of neighboring neurons. Furthermore, a given neuron could be coupled at remarkably different strengths with each of its partners. Freeze-fracture analysis of IO glomeruli revealed the close proximity of glutamatergic postsynaptic densities to connexin 36-containing gap junctions, at distances comparable to separations between chemical transmitting domains and gap junctions in goldfish mixed contacts, where electrical coupling was shown to be modulated by the activity of glutamatergic synapses. On the basis of structural and molecular similarities with goldfish mixed synapses, we speculate that, rather than being hardwired, variations in coupling could result from glomerulus-specific long-term modulation of gap junctions. This striking heterogeneity of coupling might act to finely influence the synchronization of IO neurons, adding an unexpected degree of complexity to olivary networks.

electrical synapse; connexin 36; gap junction; synaptic plasticity

GAP JUNCTION-MEDIATED ELECTRICAL SYNAPSES allow synchronization of subthreshold and spiking activity among groups of neurons (Connors and Long 2004; Bennett and Zukin 2004). In the Inferior Olive (IO), a structure where electrical transmission constitutes the only form of synaptic communication between its principal cells (De Zeeuw et al. 1998), clusters of synchronized neurons are dynamically sculpted as a result of transient regulation of electrical coupling (Llinas et al. 1974; Leznik and Llinas 2005). This regulation takes place at the glomerulus, an anatomical structure where coupled dendritic processes of IO neurons and afferent chemical synaptic contacts coexist (De Zeeuw et al. 1998). Here, release of GABA from terminals of axons originating in the deep cerebellar nuclei has been proposed to indirectly regulate coupling by shunting depolarizing currents in dendritic processes of IO neurons (Llinas et al. 1974; De Zeeuw et al. 1998). The time window of this "uncoupling" is determined by the duration of the shunting synaptic conductances, which, although unusually long due to desynchronized transmitter release (Best and Regehr 2009), last only tens of milliseconds. By promoting synchronous complex spikes that influence sets of Purkinje cells in the cerebellar cortex, these quickly and transiently formed compartments are thought to encode important functional parameters that influence the cerebellar cortex (Leznik and Llinas 2005), suggesting that the formation of groups of functionally interconnected neurons underlies essential aspects of IO function. These functional considerations generally assume that inhibitory inputs act on a network of permanently coupled IO neurons in which compartments can be sculpted.

In contrast to the mechanisms underlying fast regulation of coupling, which target the extrajunctional membrane, little is known regarding the contribution of the gap junction channels themselves to the formation of compartments of functionally coupled IO neurons. The dendrodendritic gap junctions that couple IO neurons contain channels formed by the gap junction protein connexin 36 (Cx36) (Condorelli et al. 1998). This ubiquitous neuronal connexin mediates electrical coupling between neurons in various structures including retina, hippocampal inhibitory interneurons, and thalamic relay cells (Connors and Long 2004; Bennett and Zukin 2004), where electrical synapses are reportedly regulated by various mechanisms (Urschel et al. 2006; Zsiros and Maccaferri 2008; Landisman and Connors 2005; Kothman et al. 2009). Electrical synapses formed by Cx35, a fish ortholog that shares a high degree of homology with Cx36 (O'Brien et al. 1998), were shown to be regulated by the activity of their glutamatergic counterparts at mixed synaptic contacts on the goldfish Mauthner cell (Yang et al. 1990; Pereda et al. 1998; Smith and Pereda 2003). These activity-dependent changes are terminal-specific, and as a result of this property, electrical synapses between neighboring mixed terminals coexist at various degrees of conductance, suggesting that modulation by chemical synapses is short-range and therefore constitutes a spatially restricted mechanism (Smith and Pereda 2003).

Recent evidence suggests that molecular mechanisms for the regulation of coupling that are similar to those operating in goldfish mixed synapses could also operate in the mammalian IO (Alev et al. 2008). This possibility is supported by the particular arrangement of the IO glomeruli, where electrical and chemical synapses coexist (De Zeeuw et al. 1990, 1998).

Address for reprint requests and other correspondence: A. Pereda, Dominick P. Purpura Dept. of Neuroscience, Albert Einstein College of Medicine, 1300 Morris Park Ave., Bronx, NY 10461 (e-mail: alberto.pereda@einstein.yu.edu).

As a step toward determining the contribution of gap junction channels to the formation and properties of groups of interconnected neurons in the IO, we asked whether, as they occur between mixed synapses and the Mauthner cell, *1*) electrical synapses between IO neurons coexist at various degrees of conductance, and *2*) glutamatergic synapses are located in close proximity to gap junctions in IO glomeruli. For this purpose, we combined detailed quantitative tracer-coupling analysis with paired electrophysiological recordings and freeze-fracture replica immunolabeling (FRIL). Our results indicate that, rather than forming a homogenous network, coupling in the IO is highly variable, since individual IO neurons were found coupled to a dramatically different number of other cells. Strikingly, we found that individual IO neurons are coupled at remarkably different degrees of conductance with each of their partners. FRIL analysis of IO glomeruli revealed the proximity of glutamatergic postsynaptic densities (PSDs) to Cx36-containing junctions at distances comparable to separations between chemical transmitting domains and gap junctions in goldfish mixed synapses. We speculate that these variations in coupling might result from glomerulus-specific modulation of gap junctional conductance. Heterogeneity of coupling could constitute an important regulatory property of olivary networks, determining the ability of neurons to participate in dynamically sculpted clusters and to finely influence the synchronization of their cellular activity.

MATERIALS AND METHODS

Slice Preparation

Brain stem slices (300 μm thick) were prepared from 14- to 18-day-old Sprague-Dawley rats (Charles River). Animal handling and use followed a protocol approved by the Animal Care and Use Committee of Albert Einstein College of Medicine, in accordance with National Institutes of Health guidelines. The animals were anesthetized with inhaled isoflurane, and, following decapitation, the brain stem was quickly removed and sliced parasagitally (DTK-1000 DSK Microslicer) in an ice-cold sucrose cutting solution containing (in mM) 238 sucrose, 26 $NaHCO_3$, 11 glucose, 2.5 KCl, 1 NaH_2PO_4, 1.3 $MgSO_4$, and 2.5 $CaCl_2$. Slices were then incubated for 1.5 h at room temperature in solution containing 50% of the sucrose cutting solution and 50% artificial cerebral spinal fluid (ACSF) solution containing (in mM) 119 NaCl, 26 $NaHCO_3$, 10 glucose, 2.5 KCl, 1 NaH_2PO_4, 1.3 $MgSO_4$, and 2.5 $CaCl_2$. This incubation solution was slowly replaced with ACSF to finally reach a 20% sucrose-80% ACSF composition. Both cutting and incubation solutions were saturated with 95% O_2-5% CO_2 and maintained at pH 7.4 (proper balance was obtained using small amounts of 1 M HCl or 1 M NaOH). Sliced sections were kept at room temperature until transferred to a submerged recording chamber.

Electrophysiological Recordings

Brain stem slices were placed in a recording chamber mounted on an upright microscope (Nikon E600FN), maintained at constant temperature (32°C), and perfused with oxygenated (95% O_2-5% CO_2) ACSF. Differential interference contrast (DIC) microcopy was used to visually identify IO neurons. Patch pipettes, 6–9 MΩ, were filled with internal solution containing (in mM) 0.01 EGTA, 4 NaCl, 0.001 $CaCl_2$, 10 HEPES, 140 K-gluconate, 4 Mg-ATP, and 0.6 Mg-GTP (pH 7.2, 280 mosM). Sucrose was added to correct osmolarity. For tracer-coupling experiments, 0.5% neurobiotin (NB; Vector Labs) was added to the internal solution. Recordings were obtained using a Multiclamp 700A amplifier (Axon Instruments) in current-clamp mode. IGOR Pro software (WaveMetrics) was used for data acquisition and analysis. For paired recordings, adjacent cells within 50 μm (approximately the length of the diameter of 2 cell bodies) were recorded simultaneously in current clamp. To reduce hyperpolarization-activated inward current (I_h) and thus provide more accurate estimates of the coupling coefficient, 2 mM CsCl was routinely added to the ACSF. In some experiments, the gap junction blocker meclofenamic acid (MFA; 100 μM; Sigma) was added to the ACSF.

Calculation of coupling coefficient. The strength of electrotonic coupling was estimated using measurements of steady-state coupling coefficients (*CC*). For this purpose, a current pulse of −120 to −400 pA and 250-ms duration was injected into one cell of a coupled pair and resulting voltage deflections were measured in both cells. The coupling coefficient of *cell 1* to *cell 2* (CC_{1-2}) was defined as V_2/V_1 where V_1 is the voltage deflection in the current-injected cell and V_2 is the corresponding, although attenuated, voltage deflection in the noninjected cell. Current pulses ranged from −120 to −400 pA. Averages of 60–100 traces were used to improve the signal-to-noise ratio. Only *CC* values >0.005 were considered evidence of coupling between pairs of recorded IO neurons.

Estimate of junctional conductance. Estimates of the conductance of gap junctional channels coupling IO neurons (G_j) were calculated following Bennett (1966) and Parker et al. (2009):

$$G_j = 1 \Big/ \frac{\left[\left(R_{in} cell\ 1\right) \cdot \left(R_{in} cell\ 2\right) - \left(\text{transfer resistance}\right)^2\right]}{\left(\text{transfer resistance}\right)}$$

where R_{in} represents the input resistance of the coupled cells, and the transfer resistance was defined as the voltage response in *cell 2* (when current is injected into *cell 1*) divided by the amplitude of the current step injected into *cell 1*. These estimates assume a simple two-neuron model with passive membrane properties coupled directly by a single junction and do not account for parallel conductance pathways via adjacent coupled neurons or dendritic cable properties. Because no evidence of electrical rectification was observed between pairs of IO neurons, estimates of coupling coefficient and junctional conductance are reported from voltage drops in only one direction.

Cell Labeling and Imaging

To test tracer coupling, 0.5% NB was iontophoretically injected using 500-pA pulses of 250-ms duration every second for 13–14 min. After injection, the electrode was removed and slices were incubated at room temperature for 1–2 h to allow diffusion. Slices were then fixed overnight at 4°C in 4% paraformaldehyde in 0.2 M sodium phosphate buffer (1 part sodium phosphate monobasic and 4 parts sodium phosphate dibasic; Sigma). After being washed with PBS [10× Dulbecco's PBS containing (in g/l) 1 $CaCl_2$, 2 KCl, 2 KH_2PO_4, 1 $MgCl_2 \cdot 6H_20$, 80 NaCl, and 11.5 Na_2HPO_4 was diluted to 1× and the pH adjusted to 7.4 (Cellgro Mediatech)], slices were washed in PBS containing 5% normal goat serum and 0.3% Triton and then incubated for 1 h with AlexaFluor 568-conjugated streptavidin (7.5 μg/ml, S11226; Invitrogen) in PBS containing 3% Triton. Finally, slices were washed in PBS and mounted on microscope slides for confocal analysis. Control experiments were performed by placing a NB-containing pipette under positive pressure in the extracellular space adjacent to IO neurons. The slices were then processed for NB labeling as described above.

After exposure to AlexaFluor-conjugated streptavidin, NB-labeled cells were visualized under confocal microscopy with an Olympus microscope controlled by Fluoview software. For each injected cell, 25–45 optical *z*-section images were obtained 1 μm apart to include the dendritic tree. The settings for laser power and photomultiplier tube (PMT) gain were initially set to detect all tracer-coupled cells during the confocal scans. For accurate measurements of intensity at the injected cell (which usually appears saturated), a second scan at

lower laser power and PMT gain settings was used. Because of the high concentration of NB in the injected cell, measurements of this cell's labeling intensity with lower laser power were comparable to saturated values obtained with high laser power. To maintain a uniform level of excitation and detection, both the high and low laser power settings were maintained constant for all experiments. Confocal images were analyzed off-line using basic features of ImageJ software (NIH). The intensity of labeling for each cell was estimated using the "measurement" feature of ImageJ, which provided a mean intensity value for a region of interest representing the outline of the somata. To express differences in tracer-coupling strength, an "intensity ratio" was calculated by dividing the labeling intensity of the tracer-coupled cells by the intensity of the directly labeled cell, estimated at low gain. A cell was considered coupled if the complete outline of its cell body was clearly recognizable from background. Thresholding was required to distinguish coupled somata. Digital isolation of IO neurons injected with NB was obtained from *z*-stack projection images using the "magic tool" feature of Photoshop software (Adobe). Results were expressed as average values ± standard deviation (SD) or standard error of the mean (SE). Significance of quantitative data was determined by using Fisher's exact test, the χ^2 test, and Student's *t*-test.

Freeze-Fracture Replica Immunolabeling

Two adult male Sprague-Dawley rats (158 and 496 g) were anesthetized using ketamine (80 mg/kg) and xylazine (8 mg/kg), fixed by perfusion with 1% formaldehyde in Sorenson's phosphate buffer (pH 7.4), and decapitated. The brain stem was removed and transversely sliced at 150 μm using a refrigerated Lancer Vibratome 3000 (Technical Products International, St. Louis, MO) that maintained samples at 4°C. One goldfish was prepared for FRIL, as described in Pereda et al. (2003a), and portions of that sample were previously described. Samples of rat IO were frozen, and freeze-fracture replicas were made according to our published methods (Rash and Yasumura 1999). (However, in one replica made in 1999, during modification and testing of our freeze-fracture machine, Pt was applied continuously rather than in short bursts, resulting in slightly larger grain size and lower specimen contrast in one sample, as described below.) A gold "index" grid containing a drop of 1.5% Lexan dissolved in dichloroethane was placed on the frozen sample, and the solvent was allowed to evaporate overnight at −25°C. The replicated tissue/Lexan/gold grid "sandwiches" were thawed and photomapped by confocal microscopy using tissue autofluorescence. Bulk tissue was removed from the Lexan-stabilized replicas by washing in 2.5% SDS detergent in Tris·HCl buffer (pH 8.9) for 22 or 27 h at 40 or 47°C. This washing procedure leaves a thin film of lipid and protein molecules adhering to the highly absorptive platinum-carbon replica (Fujimoto 1995), plus additional molecules that are bound to the molecules that are directly adsorbed to the replica (Fujimoto 1995; Rash and Yasumura 1999). SDS-washed replicas were rinsed in "blocking buffer" [10% heat-inactivated goat serum and 1.5% fish gelatin in Sorenson's phosphate buffer, pH 7.4 (Dinchuk et al. 1987)] and labeled for 60–220 min using rabbit polyclonal antibodies to Cx36 [Ab298 (Rash et al. 2000; Pereda et al. 2003a); from Dr. James Nagy, University of Manitoba, Winnipeg, Canada] with or without monoclonal antibodies to glutamate receptor subunit NR1 (Ab55-6308; BD Biosciences PharMingen, San Diego, CA). Replicas of goldfish Mauthner cells were labeled using polyclonal antibody Ab298 and monoclonal antibodies to NR1 (both as described above). Labeled samples were rinsed and counterlabeled using goat anti-rabbit IgG and goat anti-mouse IgG, each coupled to a separate size of uniform-diameter gold beads [10 or 20 nm (Chemicon, Temecula, CA; secondary immunogold antibodies no longer available from Chemicon); 6, 12, and 18 nm (Jackson ImmunoResearch Laboratories); and 10 or 30 nm (BBInternational, Cardiff, UK; obtained from Ted Pella, Redding, CA)]. After immunogold labeling, each sample was air-dried and coated on the labeled side with 10–20 nm of evaporated carbon to anneal temperature-induced stress cracks in the replica, as well as to stabilize the immunogold beads. The Lexan support film was removed by immersing the grids in ethylene dichloride solvent for 1–2 h and was then air-dried.

Electron Microscopy

FRIL samples were examined in a JEOL 2000 EX-II transmission electron microscope (TEM), and stereoscopic images (8° included angle; tilt range ±60°) were obtained at TEM magnifications from ×10,000 to ×100,000. Negatives were digitized using an ArtixScan 2500f digital scanner (Microtek, Carson, CA) and processed using Photoshop 7.01 (Adobe). Stereoscopic images were used to assess complex three-dimensional membrane topography, as well as to confirm that each label was on the tissue side of the replica. [Relatively rare nonspecific binding is primarily on the Lexan-coated side of the replica (Rash and Yasumura 1999)]. Neurons and glia were identified in freeze-fracture replicas on the basis of 24 inclusive and exclusive criteria described by Rash et al. (1997). For neurons, these included the presence of >25 uniform-diameter synaptic vesicles in nerve terminal cytoplasm, pre- and postsynaptic membrane specializations called active zones and PSDs, and absence of glial cell markers (glial fibrillary acidic protein filaments, aquaporin-4 square arrays, etc.). Gap junctions were identified using well-established criteria (reviewed in Rash et al. 1998a), including *1*) uniform 8- to 9-nm-diameter intramembrane particles (IMPs) in replicated protoplasmic leaflets ["P faces"; the internationally recognized freeze-fracture terminology of Branton et al. (1975) is used in this report] and uniform 8- to 9-nm-diameter pits in the extraplasmic leaflet (E face); *2*) close packing of IMPs/pits, often in hexagonal array; *3*) narrowing of the extracellular space within the border of the gap junction; and *4*) maintained alignment of IMPs and pits across the step from E to P face. In addition, immunogold labeling for Cx36, restricted to gap junctions only in neurons, was considered confirmatory evidence.

RESULTS

Confocal Analysis Reveals a High Incidence and Variability of Tracer Coupling

We investigated the variability of coupling between IO neurons by combining tracer coupling with fluorescence confocal microscopy analysis. Unlike whole cell recordings, which restrict the analysis to pairs of neurons, tracer-coupling analysis permits simultaneous evaluation of the degree of coupling between a given IO neuron and all its coupled partners. To this end, brain stem slices containing the inferior olivary nucleus (Fig. 1*A*) were prepared and IO neurons were identified with DIC optics (Fig. 1*B*, *inset*) for whole cell patch-clamp recordings with electrodes containing NB, a tracer molecule permeant to gap junctions. Most of the recorded cells (~85%) were located in the central region of the principal olive, whereas fewer were located in the dorsal olive. IO neurons were identified by their electrophysiological properties, consisting of a characteristic I_h sag in response to hyperpolarizing current injection that triggers an action potential, immediately followed by a prolonged afterdepolarization, which is terminated by a pronounced afterhyperpolarization (Llinas and Yarom 1981; Bal and McCormick 1997) (Fig. 1*B*). After NB injection, the recording pipette was removed and slices were incubated to allow diffusion of NB. Slices were then processed with AlexaFluor 568-conjugated streptavidin to label NB-containing cells for their anatomical identification and analysis

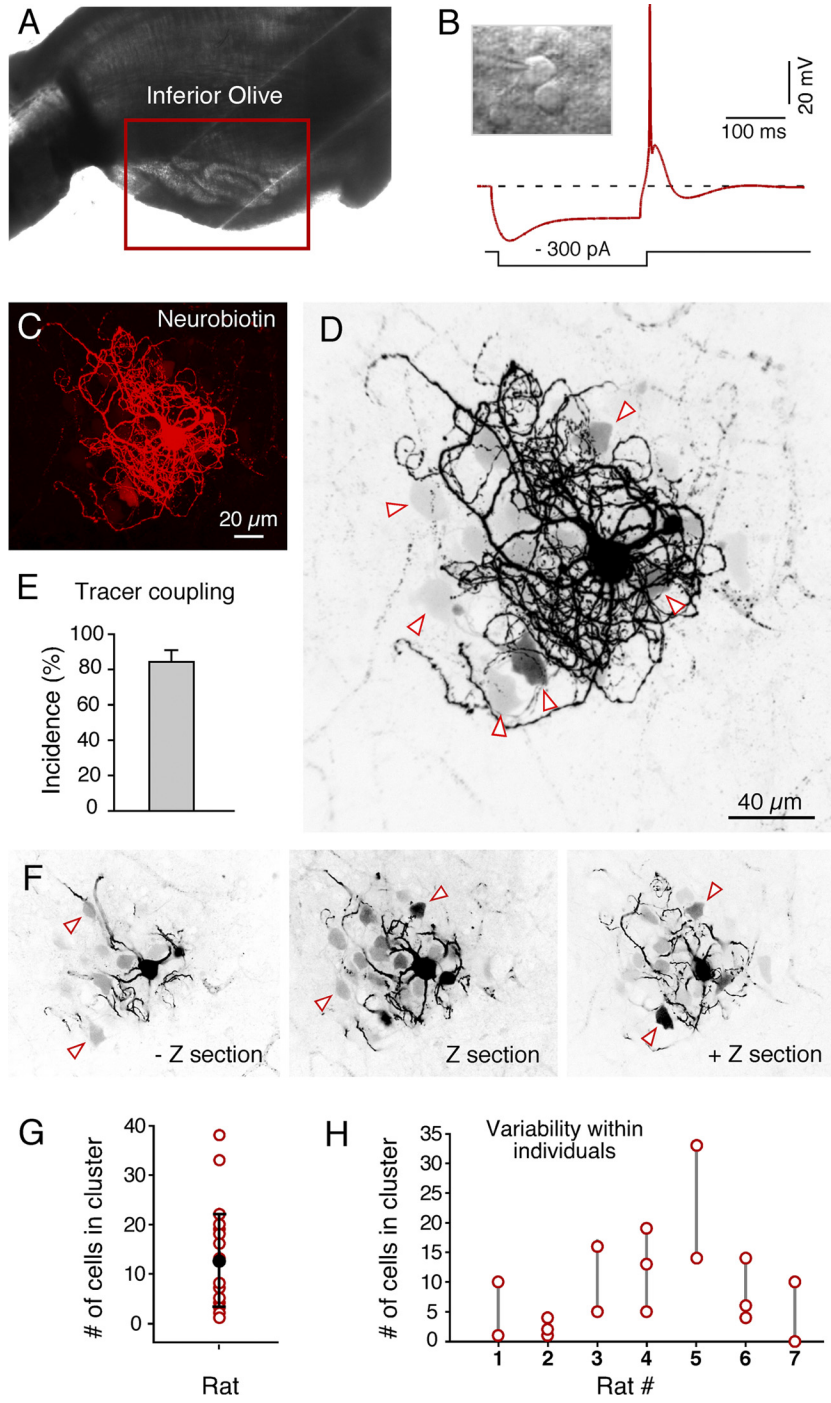

Fig. 1. Confocal microcopy reveals high incidence of tracer coupling in the inferior olive (IO). *A*: parasagittal brain stem slice showing the IO. *B*: whole cell recording of an IO neuron (*inset*) showing a characteristic electrophysiological response to a hyperpolarizing current pulse (−300 pA, 300 ms). *Inset*: differential interference contrast (DIC) image shows the recording of a IO cell. *C*: confocal image of an IO neuron in which neurobiotin (NB) was injected during a whole cell recording and revealed afterward with AlexaFluor 568-conjugated streptavidin (maximum intensity projection). Note the complex dendritic arborizations, characteristic of a "curly" type IO neuron. The image represents a confocal reconstruction (*z*-stack projection composed by 40 single images). Indirectly labeled neurons are visible within the proximity of the dendritic tree. *D*: the fluorescent image from *C* was converted to grayscale and inverted for better visualization and analysis of indirectly labeled (tracer coupled) cells (arrowheads). *E*: bar graph summarizes confocal microscopy analysis, revealing that 27 of 32 NB-injected neurons showed at least 1 indirectly labeled cell (incidence 84%). *F*: 3 subsequent optical *z*-sections, 5 μm apart, obtained using confocal microscopy show tracer-coupled cells visible at different focal planes (arrowheads). This approach was used to estimate both the number of coupled cells and the maximum labeling intensity of each coupled cell at the corresponding *z*-section. *G*: graph summarizes the number of tracer-coupled cells observed in each experiment. This number was highly variable, ranging from 1 to 38 (red circles) and averaging 12.5 ± 1.8 SE. *H*: graph shows the variability of the number of coupled cells in slices from 7 different rats. Injected neurons (red circles) exhibit a high variability in the number of coupled cells within each animal (1–7).

with confocal microscopy (Fig. 1, *C*, *D*, and *F*). In all cases, the injected cells were unambiguously identified as IO neurons because of their size and characteristic dendritic morphology. Most of these cells (~90%) had anatomical features characteristic of "curly" IO neurons, whereas only 3 of the 32 injected cells showed "straight" dendritic morphology. In contrast to a previous report (Devor and Yarom 2002), our approach revealed a high incidence of coupling in the IO, where at least one tracer-coupled cell was detected for 27 of the 32 injected neurons (incidence 84%) (Fig. 1*E*). Notably, the number of tracer-coupled cells was highly variable, ranging from 1 to 38 cells, averaging 12.5 ± 1.8 SE (Fig. 1*G*). Such variability in the number of coupled cells was also observed within the same animal (Fig. 1*H*) and even within the same slice (not shown), where clusters of coupled cells dramatically differed in size, suggesting that the observed variability cannot be ascribable to subtle differences in experimental conditions between experiments. Although we restricted our quantitative analysis to curly neurons to avoid potential differences between cell types, tracer coupling was also observed in "straight" neurons (see below). Unfortunately, because dendritic morphology was not evident in tracer coupled cells, we were unable to determine whether coupling specifically occurs only between curly or between straight neurons or whether it could also occur heter-

ologously between these two types of neurons. Thus our data showed that although coupling between IO neurons seems prevalent (~85%), the number of cells in these clusters of coupled IO neurons was highly variable.

Labeling of IO Cells is Mediated by Gap Junctions

We carried out control experiments to unambiguously establish that the observed cell labeling corresponded to coupling via gap junction channels. First, to rule out the possibility that labeling of noninjected cells resulted from extracellular accumulation of NB as a result of leakage from the recording electrode during the formation of the patch, we compared intracellular and extracellular applications of NB. Both dark and faint somata labeling were only detected when NB was injected intracellularly in IO neurons (Fig. 2*A*). In contrast, puffing of the NB-containing internal solution into the extracellular space for about 4 min resulted in labeling of blood vessels only (Fig. 2*B*), which exhibited affinity for this tracer. Second, experiments using the gap junction blocker MFA (Pan et al. 2007; Veruki and Hartveit 2009) indicated that cell labeling was indeed gap junction mediated. Brain stem slices containing the IO were incubated for at least 40 min with MFA (100 μM) before NB injection into IO neurons. This pretreatment greatly reduced the incidence of tracer coupling to 36% compared with 89% in untreated slices harvested from the same animals ($n = 11$ and $n = 9$ injected cells, respectively; $P = 0.024$, Fisher's exact test) (Fig. 2*C*). MFA pretreatment also decreased the number of coupled cells. Only 5 coupled cells were identified from 11 pretreated injected neurons (averaging 0.82 ± 0.46 SE) compared with 92 from 9 untreated injected cells (averaging 10.2 ± 3.3 SE; $P < 0.01$, Student's *t*-test) (Fig. 2*D*). Incubation with MFA (40 min, 100 μM) also reduced the likelihood of finding pairs of electrically coupled cells during paired whole cell recordings (10%, compared with 81% of adjacent cell pairs in untreated slices, $P = 0.000021$, Fisher's exact test; also significant with the χ^2 test, $P < 0.001$) (Fig. 2, *E* and *F*), independently confirming that MFA effects were mediated by acting on gap junction channels. Together, these results suggest that NB labeling of noninjected cells does not result from surface cell labeling or its uptake from the extracellular space but from diffusion through NB-permeable gap junctions.

Coupling Between a Given IO Neuron and Each of Its Partners is Highly Variable

Strikingly, we found that the intensity of labeling of the tracer-coupled cells was highly variable. The observation and quantification of this variability was facilitated by our experimental approach, which relied on confocal microscopic examination and measurement of maximum fluorescence at each coupled cell. An example of this analysis is illustrated in Fig. 3*A*, where a confocal reconstruction of a NB-injected IO neuron and tracer-coupled somata is shown. The injected IO neuron (curly type) was digitally isolated (Fig. 3*B*), and the fluorescence of each of the 13 coupled cells, represented by the outline of their somas (Fig. 3*C*), was measured at the confocal section that showed maximum intensity (expressed as the various shades of gray in Fig. 3). To express the variability of coupling, we created a ratio between the labeling intensity

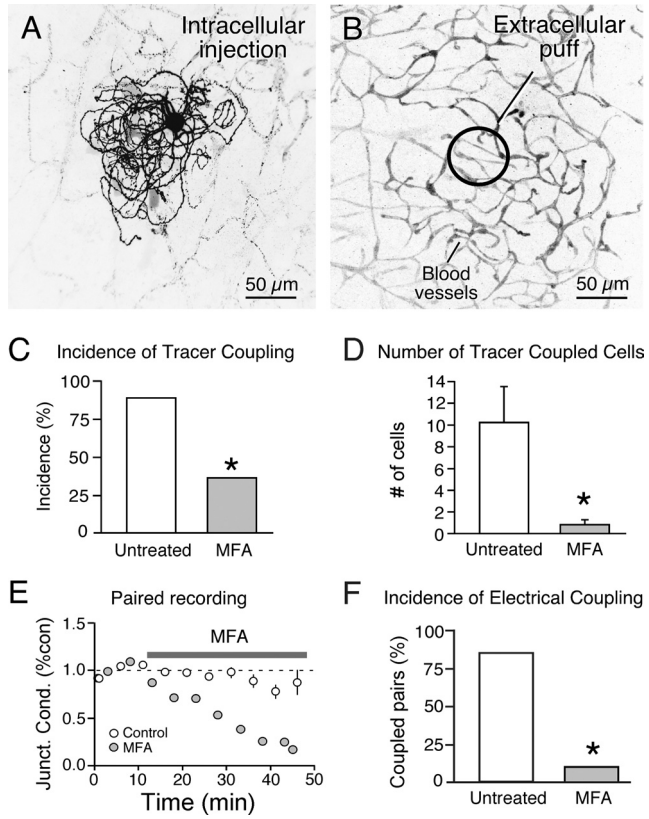

Fig. 2. Gap junctions mediate cell labeling. *A*: intracellular injection of NB-labeled IO cell bodies and dendrites and other labeled neuronal somata. Some blood vessels appear faintly labeled as a result of leakage of NB in the extracellular space before formation of the whole cell patch. *B*: extracellular application of NB does not label somata. A recording pipette containing NB was placed in the extracellular space of a similar area of the principal olive while positive pressure (of magnitude similar to that used for patching) was applied for 5 min. Although this manipulation resulted in strong labeling of blood vessels, no labeled somata were detected despite examination with higher laser power and the high density of IO neurons (density estimated in 5×10^4 cells/mm^3; Devor an Yarom 2002). *C*: incubation (40–60 min) with the gap junction blocker meclofenamic acid (MFA; 100 μM) reduced the incidence of tracer coupling: only 4 of 11(36%) MFA-treated cells showed tracer coupling compared with 8 of 9 untreated injected cells (89%). *$P < 0.024$, Fisher's exact test. *D*: MFA pretreatment also reduced the number of tracer-coupled cells, averaging 0.82 ± 0.46 SE ($n = 11$ injected cells) compared with that observed in control slices, 10.2 ± 3.3 SE ($n = 9$ injected cells). *$P < 0.01$, Student's *t*-test. *E*: application of MFA (100 μM) dramatically reduced junctional conductance (Junt. Cond.) in a pair of electrically coupled IO neurons (control represents an average of 3 long-lasting recordings). *F*: the incidence of electrical coupling between pairs of adjacent IO neurons averaged 81 ± 4.5% ($n = 77$ cell pairs) and was dramatically reduced in slices pretreated with MFA (>40 min, 100 μM), averaging 10 ± 3.2% ($n = 10$ cell pairs). Values are means ± SE. *$P = 0.000021$, Fisher's exact test.

for each cell and the intensity of the directly injected neuron. This intensity ratio (see MATERIALS AND METHODS), conceptually comparable to coupling coefficients in paired recordings (although coupling coefficients are measured at steady-state conditions), allowed us to quantify differences between tracer-coupled cells. The distribution of the intensity ratios for this particular IO neuron is illustrated in the histogram of Fig. 3*D*, showing that the degree of coupling of this neuron with its partners was highly variable. This variability of coupling was not specific to curly neurons,

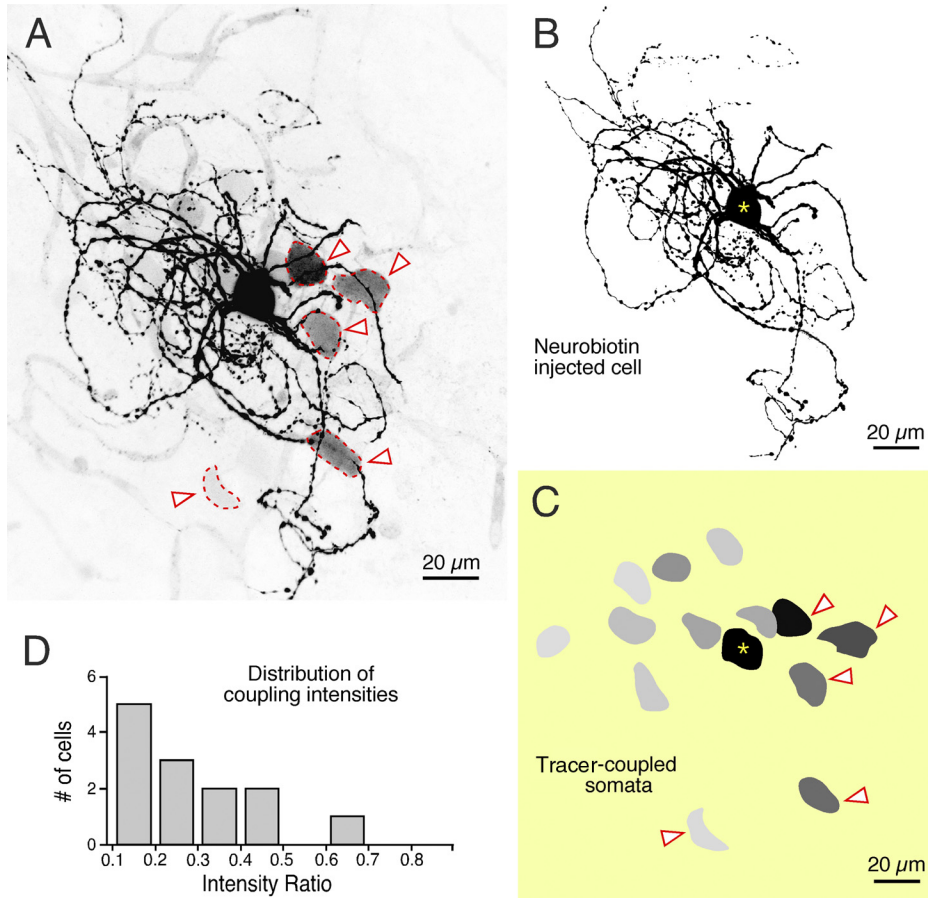

Fig. 3. Labeling intensity of the somata of coupled cells is highly variable. *A*: image corresponds to a confocal projection (average of 17 *z*-sections) illustrating a NB-injected IO neuron with multiple indirectly labeled cells. *B*: the injected cell in *A* was isolated by image analysis using confocal reconstruction. *C*: reconstruction of the somata of tracer-coupled cells in *A*, using confocal analysis. The contour of the somata and the intensity of the labeling (represented by the different shades of gray) were obtained at the *z*-section in which labeling was most intense; darker silhouettes represent brighter fluorescence labeling (asterisk indicates the injected cell). Injected neurons, i.e. maximum intensity, is indicated by solid black areas, whereas coupled somata are represented by shades of gray corresponding to their relative intensity. Arrowheads denote cells in the reconstruction that can also be observed in the confocal projection in *A*. Yellow background is used to enhance comparison of the various shades of gray. *D*: histogram shows the differences of labeling intensity for the coupled cells in *A*, expressed as an "intensity ratio" (intensity of tracer-coupled neuron divided by intensity of the NB-injected neuron; see MATERIALS AND METHODS).

since similar variability was observed in straight neurons (Fig. 4).

Tracer-Coupling Labeling Intensity is Not Correlated With Distance

Variability of labeling intensity in tracer-coupled cells was observed in other structures, such as the retina (Mills and Massey 1998), and in cell cultures (Cusato et al. 2003), where secondary tracer coupling (transfer of tracer from a primarily coupled neuron to a secondary neuron and so forth) was documented. In these cases, labeling intensity was found to be a function of distance from the originally tracer-containing coupled cells (Mills and Massey 1998). To investigate the possibility that the observed variability of labeling results from secondary coupling between IO neurons, we correlated the labeling intensity of coupled neurons with the distance between their somata and the NB-injected neurons. We found that the labeling intensity of the coupled neurons was not correlated with the distance from the NB-injected cell. That is, both darkly and faintly labeled somata were located at widely different distances from the injected IO neurons (see Figs. 3, 4, 5, and 6*A*). This finding is illustrated in Fig. 5, in which star plots that graphically code for intensity (shade of gray) and distance (length) were constructed for five different injected IO neurons (*A* and *D–G*). As can be appreciated in the example illustrated in Fig. 5*A*, in which an IO neuron was coupled to 35 neighbors, the labeling intensities of the coupled somata were not correlated with their distance from the injected cell, despite the wide variability of labeling intensity (Fig. 5*B*; see also Fig. 5, *D–G*, for the other examples). As expected, the intensity ratio for the total population of IO neurons was also highly variable (Fig. 5*C*) and was not correlated with the distance between somata of the coupled cells and the NB-injected cell (Fig. 5*H*), suggesting that the variability of labeling intensity observed in coupled cells is unlikely to result from secondary tracer coupling. Finally, tracer coupling almost exclusively occurred within the dendritic tree of the injected neuron (where contacts are made), suggesting that all of the labeled cells were directly coupled (primary coupling). Only 4 of the 338 cells in which the tracer was detected were located outside the dendritic tree of the injected neuron. These four cells were located very close to labeled dendrites (less than ~50 μm) and thus perhaps within the range of smaller, undetected, dendritic processes. Furthermore, this distribution was independent of the cell type and the extent of the dendritic tree, which is almost twice as large in straight neurons (compare Figs. 3*A* and 4).

Paired Recordings of IO Neurons Show High Variability of Electrical Coupling

Analysis of tracer coupling suggested that coupling between IO neurons was highly variable. To independently confirm this variability, we performed paired whole cell recordings from somas of adjacent neurons that were within a <50-μm-diameter area, within which we observed a high variability in tracer-coupling labeling intensity (Fig. 6, *A* and *B*). We also observed a wide variability of electrical coupling between

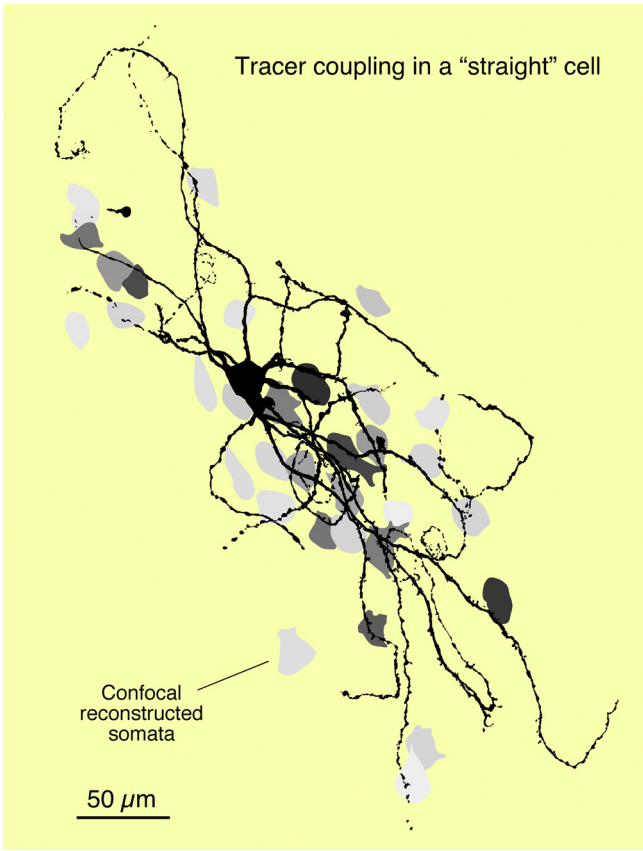

Fig. 4. Tracer coupling in a "straight" IO neuron. The image corresponds to the confocal reconstruction of a NB-filled neuron with straight dendritic morphology (image represents an average of 43 *z*-sections). The contour of the somata of the tracer-coupled neurons was also reconstructed, and their corresponding labeling intensities appear represented by the different shades of gray (darker cells represent brighter fluorescence labeling).

adjacent IO neurons where pairs with low (Fig. 6*C*) and high (Fig. 6*D*) coupling coefficients coexist. This striking diversity of electrical coupling illustrated by the distribution of estimates of junctional conductance (Fig. 6*E*) was obtained for each pair of IO neurons ($n = 91$ cell pairs). Thus both tracer and electrical coupling were highly variable between neighboring IO neurons.

Although measurements of electrical coupling are consistent with the variability observed in tracer-coupling analysis, they were obtained by measuring pairs of IO neurons, an approach that does not reveal differential coupling (i.e., differences in coupling between a given neuron and its partners) because it only examines two neurons at a time. To more conclusively establish the variability of electrical coupling between IO neurons, we performed sequential paired recordings between a given IO neuron and some of its partners (Fig. 7). For this purpose, after measuring electrical coupling between a pair of adjacent IO neurons, one of the pipettes was removed and recordings from different adjacent neurons, located within a 50-μm radius, were sequentially obtained while the recording pipette was held in the other cell. This approach allowed us *1*) to directly establish the variability of electrical coupling between a given IO neuron and its coupled partners and *2*) to correlate the strength of electrical coupling with the distance between their somata (Fig. 7*A*). In all cases, recordings were stable and no significant changes in the input resistance of the holding cell were detected during the sequential recordings (input resistance measurements stayed within 15% of their original values). As observed in Fig. 7, *A* and *B*, the strength of coupling could be markedly different between immediate neighbors and was not correlated with the distance between the recorded cells. Similar results were observed in three other examples (Fig. 7, *C–E*). Finally, as with intensity ratios in tracer-coupling experiments, the strength of electrical coupling (expressed as junctional conductance) was not correlated with the distance between somata in these paired recordings (Fig. 7*F*). Thus, although a given IO neuron can be electrically coupled to multiple neurons, the strength of coupling was different in each case.

Proximity of N-Methyl-D-Aspartate Receptor-Containing Postsynaptic Densities to Gap Junctions in IO Glomeruli

The observed coupling variability could be due to differences in the size of gap junctions coupling the cell processes of a given IO neuron with each of its partners. Alternatively, it could result from differential regulation of gap junction channels at IO glomeruli. Spatially restricted *N*-methyl-D-aspartate receptor (NMDAR)-dependent regulation of gap junctions that requires downstream activation of Ca^{2+}-calmodulin-dependent kinase II (CaM-KII) was shown to occur at goldfish mixed synapses (Yang et al. 1990; Pereda and Faber 1996), where NMDAR-containing PSDs are located in close proximity to Cx35-containing gap junctions (Smith and Pereda 2003) (Fig. 8*A*). Because modulation of electrical transmission at these mixed synapses occurs postsynaptically (Pereda et al. 1998), the interactions may not be only limited to mixed synapses but are likely found where chemical synapses are close to gap junctions formed by different presynaptic elements. Recent reports indicate that CaM-KII colocalizes with Cx36 in the IO (Alev et al. 2008) and with Cx35 in goldfish mixed synapses (Flores et al. 2010), suggesting that similar mechanisms could operate at these gap junctions. Given the convergence of chemical and electrical synapses in the IO glomerulus, we examined whether glutamatergic PSDs are located close to gap junctions using FRIL double-immunolabeling. We observed E-face particle aggregates close to dendrodendritic gap junctions containing Cx36 in IO glomeruli at distances comparable to separations between chemical transmitting domains and gap junctions in goldfish mixed synapses (~0.2–0.3 μm; Pereda et al. 2003a,b) (Fig. 8*B*). Figure 8*C* illustrates the proximity of one of these E-face particle aggregates that is associated with a presynaptic process (probably a glutamatergic terminal) in close proximity to a gap junction formed by two other processes, which likely correspond to spines of IO neurons. These E-face particle aggregates are known to correspond to glutamatergic postsynaptic densities (Harris and Landis 1986), as confirmed by immunogold antibodies directed against the NR1 subunit of the NMDA receptor (Fig. 8, *B* and *D*). These PSDs were labeled by only a small number of immunogold beads, which is expected because NMDA receptors constitute only a small fraction of the glutamate receptors present at PSDs (Takumi et al. 1999). Thus ultrastructural analysis indicates that gap junctions and glutamatergic synapses containing NMDARs, a key element for regulation of coupling at goldfish mixed synapses (Yang et al. 1990; Pereda and Faber 1996), coexist in IO

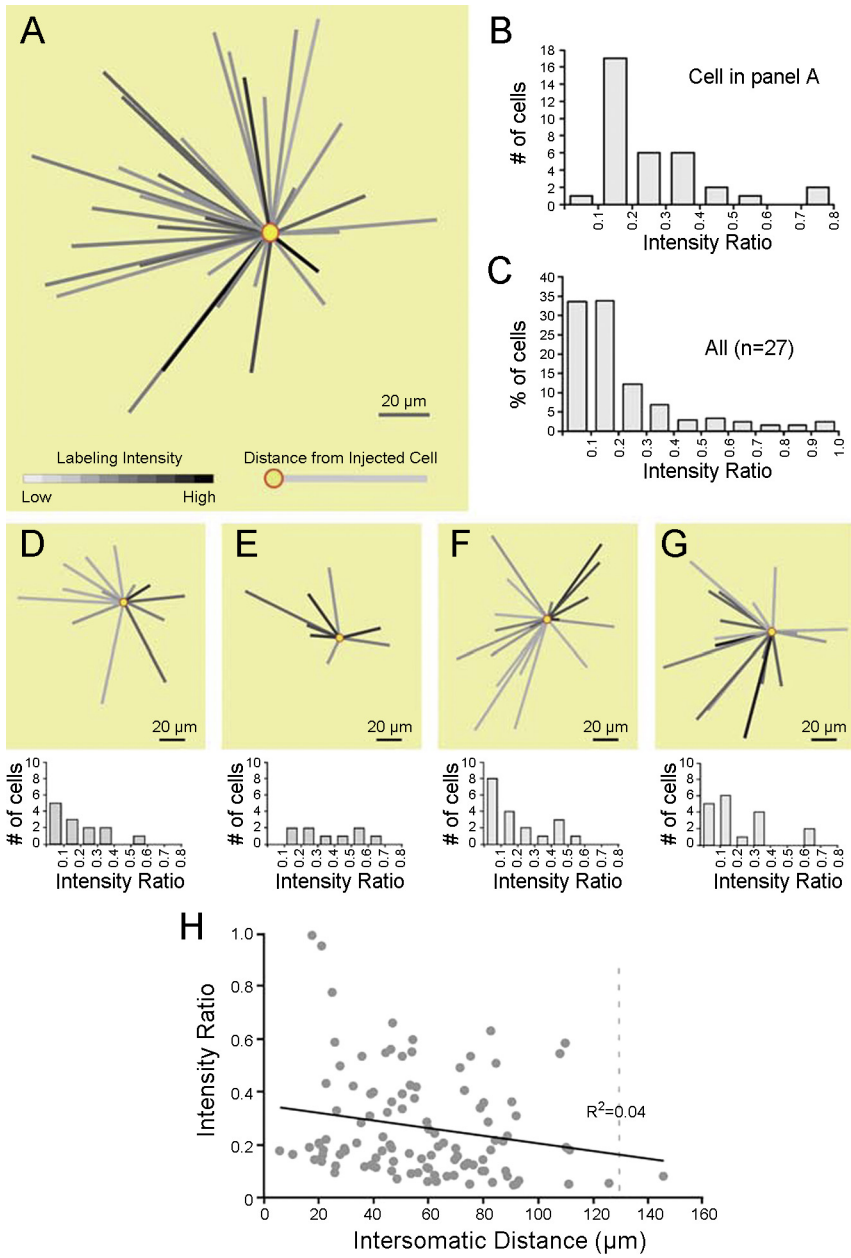

Fig. 5. Labeling intensity of coupled somata is not correlated with the relative distance from the NB-injected neuron. The intensity of labeling of tracer-coupled somata was not correlated to their distance from the injected IO neuron, suggesting that a difference in labeling does not correspond to secondary coupling. *A*: relative location (length) and labeling intensity (shade of gray) of tracer-coupled neurons in the example shown in Fig. 1*D* are represented as a star plot. The angle of display of each line was arbitrarily chosen to optimally illustrate the variability of labeling and distance. *B*: histogram summarizes the intensity ratios estimated for the cell illustrated in *A*. *C*: histogram shows the intensity ratios estimated for all the observed tracer-coupled cells (338) observed in the 27 experiments where coupling was detected. *D–G*: star plots and intensity histograms for 4 other examples. As with the example in *A*, the labeling intensity of tracer-coupled somata was not correlated with their distance from the injected IO neurons. *H*: graph plots the relative distance vs. labeling intensity for the coupled cells illustrated in *A–G* (n = 111 cells). Again, there was no correlation between labeling intensity and the distance of the somata from the injected IO neuron, as indicated by least-squares regression analysis (R^2 equals the square of the correlation coefficient between the observed and predicted data values). The dotted line represents the longest dendritic process measured in these 5 examples, indicating that most of the tracer-coupled neurons occurred within the dendritic field of individual IO neurons.

glomeruli at distances where functional interactions can take place.

DISCUSSION

IO Neurons are Heterogeneously Coupled

We report in this study that coupling between IO neurons is highly heterogeneous. The analysis of variations in coupling was facilitated by a sensitive technique that takes advantage of confocal microscopy for accurate detection of tracer coupling. By virtue of its three-dimensional nature, this confocally based approach enhanced detection and revealed a higher incidence of tracer coupling compared with a previous analysis that relied on DAB staining and conventional microscopy and was therefore restricted to two-dimensional analysis (Devor and Yarom 2002). Such enhanced detection reduced the ambiguity in the identification of coupled cells and optimized the measurement of labeling intensity. This approach allowed us to reveal an unexpected high variability of coupling between IO neurons, which ranged from apparently "noncoupled" to coupling with up to 38 other IO neurons. Furthermore, by combining quantitative tracer-coupling analysis and electrophysiological approaches, we have demonstrated that the degree of coupling between a given IO neuron and each of its partners is surprisingly heterogeneous. The observed variability of coupling cannot be ascribed to secondary coupling (from primary to secondary labeled neurons and so forth) that was detected in other structures (Mills and Massey 1998) because the intensity of tracer-coupling labeling was not correlated with distance from the injected cell, a finding that was independently confirmed during sequential recordings from pairs of IO neurons. Although when compared with other brain regions the anatomical arrangement of the IO is less favorable for detecting

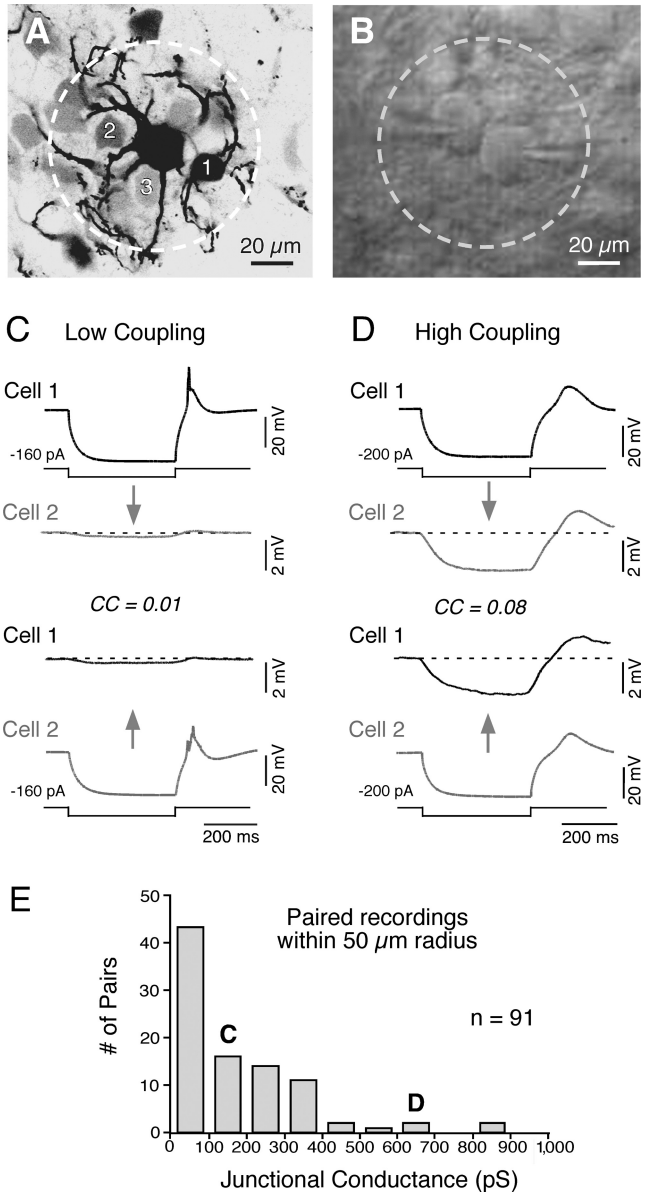

Fig. 6. Paired recordings from pairs of adjacent IO neurons show high variability of electrical coupling. *A*: tracer coupling is variable in adjacent cells (<50 μm). Despite our finding that the somata of *cells 1*, *2*, and *3* are located at comparable distances from the injected neuron, they exhibit dramatically different degrees of labeling. *B*: paired recordings made from adjacent IO neurons (DIC image). Circle represents the 50-μm-radius area where variable tracer coupling was routinely observed. *C* and *D*: electrical coupling was investigated with pulses of hyperpolarizing current; hyperpolarizing pulses in "presynaptic" cells can be detected as coupling potentials of similar time course but dramatically smaller amplitude in "postsynaptic" cells. *C* shows bidirectional electrical transmission in a weakly coupled pair, and *D* shows an example of a strongly coupled pair, and their locations are indicated in *E*, a histogram of estimates of junctional conductance obtained for a total of 91 pairs of adjacent IO neurons, obtained at intersomatic distances <50 μm. The distribution of strengths of electrical coupling between pairs of IO neurons shows high variability.

secondary coupling, if secondary labeling were a significant component of the observed diversity of coupling, we would have expected that the labeling intensity of coupled somata would have shown at least weak correlation with the distance from the NB-injected cell. Rather, heterogeneity of both tracer and electrical coupling almost exclusively took place within the dendritic tree of the injected neuron (where contacts are made), suggesting that all of the labeled cells were directly coupled (primary coupling). Although measurements of electrical coupling are likely to be more sensitive, since tracer coupling has been reportedly undetected in some networks of electrically coupled neurons (Gibson et al. 1999), tracer and electrical coupling observations were similar in our study, and both revealed a high variability in coupling strength. Nevertheless, although more sensitive than previous approaches, our measurements of tracer coupling are likely to represent an underestimate of the total number of coupled cells (estimated to be ~50, based on estimates of neuronal density; Devor and Yarom 2002), because the tracer could exist at levels below our threshold of detection in some neurons. Secondary coupling, which must exist, is also likely to be below our level of detection. Heterogeneity of coupling between an IO neuron and its partners was observed in virtually all of the explored cells, both the curly and straight types, and therefore is likely to constitute a widespread property of neurons across the principal olive. Thus, although the properties of electrical coupling in the IO were explored in previous studies (Devor and Yarom 2002; Leznik and Llinas 2005), which reported the existence of some variability in tracer and electrical coupling, our study differs from those previous reports in that it specifically focused on unambiguously establishing the existence and properties of the variability of coupling between IO neurons. Since loss of electrical coupling in Cx36-deficient animals has a profound effect in the synchronization of inferior olivary cells (Long et al. 2002, Van Der Giessen et al. 2008), the variabilities in strengths of these electrical connections are likely to be functionally relevant.

On the Origin of Coupling Heterogeneity

A simple interpretation regarding the origin of coupling diversity could be that it results from differences in the number of gap junction channels linking dendritic processes within IO glomeruli. The notion that coupling heterogeneity might be hardwired constitutes a distinct possibility. An alternative interpretation, more consistent with current views regarding mechanisms of brain function (Marder and Goaillard 2006), is that this variability reflects dynamic aspects of olivary networks. The possibility that the observed heterogeneity of coupling between a given IO and its partners results from a spatially restricted regulation of gap junctions is supported by the example of goldfish mixed synapses. At those terminals, gap junctions are regulated by the activity of the glutamatergic synapses localized within the same contact, creating a wide diversity of coupling between individual terminals and the lateral dendrite of the Mauthner cell (Smith and Pereda 2003). The regulatory mechanism requires NMDAR activation and downstream activation of CaM-KII (Yang et al. 1990; Pereda and Faber 1996; Pereda et al 1998; reviewed in Pereda et al. 2004). Because induction of modulation of electrical coupling at goldfish mixed synapses occurs postsynaptically (Pereda et al. 1998), short-range functional interactions may not be limited only to mixed synapses but may be found where glutamatergic synapses are close to gap junctions formed by other presynaptic elements. Consistent with this possibility, our FRIL analysis revealed the proximity of NR1-containing PSDs to Cx36-containing gap junctions at distances comparable to

separations between the chemical transmitting domains and gap junctions in goldfish mixed synapses, suggesting that similar interactions between electrical and glutamatergic synapses might occur in the IO. Several lines of evidence also support this possibility: *1*) Cx36 and Cx35 are highly homologous and share regulatory sequences for CaM-KII (Flores et al. 2010); *2*) CaM-KII has been shown to colocalize with both Cx36 in the IO (Alev et al. 2008) and Cx35 in goldfish mixed synapses (Flores et. al 2010); *3*) CaM-KII associates with both Cx36 (Alev et al. 2008) and Cx35 (Flores et al. 2010); and *4*) the association of CaM-KII with Cx35 is believed to be indicative of the degree of potentiation of electrical transmission at goldfish mixed synapses (Flores et al. 2010). Interestingly, a recent report suggests that the drug modafinil, an antinarcoleptic and mood-enhancing drug, might enhance electrical coupling between IO neurons through a mechanism that requires the activation of CaM-KII (Urbano et al. 2007). Glutamatergic transmission was also shown to promote activity-dependent long-term depression of electrical coupling between the inhibitory neurons of the rat thalamic reticular nucleus via activation of metabotropic glutamate receptors in this case (Landisman and Connors 2005), providing a potential mechanism for bidirectional control of electrical coupling. Thus, although GABAergic terminals originating in the deep cerebellar nuclei promote transient decoupling by acting on the nonjunctional membrane at IO glomeruli (Llinas et al. 1974), our work raises the possibility that excitatory terminals of mesodiencephalic origin (De Zeeuw et al. 1990, 1998) could act to promote more lasting modifications of electrical coupling via activation of glutamate receptors (Fig. 8). Future studies are necessary to obtain functional evidence for the existence of such mechanisms. Supporting this possibility, a recent report suggests that Cx36 phosphorylation can vary locally (Kothmann et al. 2009).

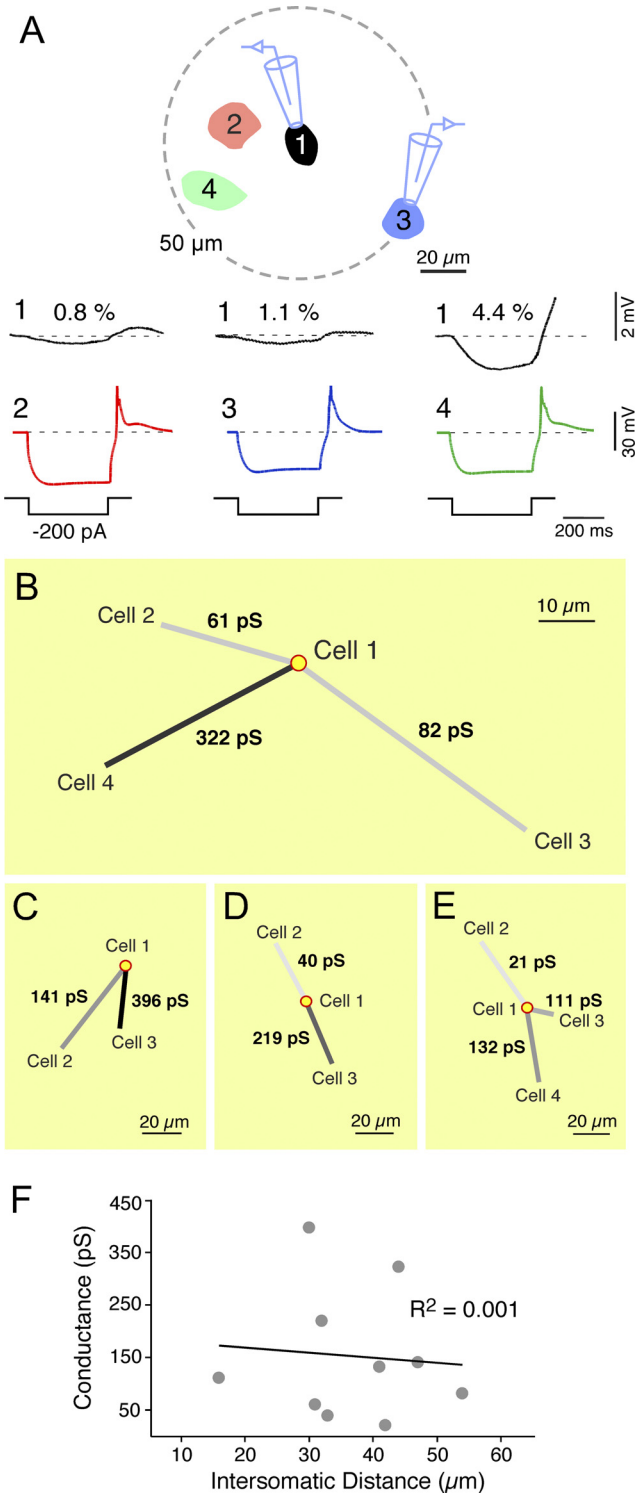

Fig. 7. Sequential paired recordings between a given IO neuron and adjacent partners reveal variability of electrical coupling. *A*: diagram illustrates paired recordings made between a given IO neuron (*cell 1*) and 4 neighboring neurons within a 50-μm radius (*cells 2–4*); recordings in the neighboring neurons were obtained sequentially while maintaining the recording in *cell 1*. The input resistance of *cell 1* remained stable throughout the experiment (within 15% of original values). *Top* traces (black) show the voltage deflection (coupling potential) obtained in *cell 1* when *cell 2*, *3*, or *4* (*middle* trace, colors) were injected with hyperpolarizing current pulses. As shown, the strength of electrical coupling was not the same in each recording, and it was not correlated with the distance of the recorded cell respective to *cell 1*. *Bottom* trace shows the recording protocol. *B*: the relative location and junctional conductance for the 3 pairs illustrated in *A* are represented as a star plot. *C–E*: star plots for 3 other examples of sequential paired recordings showing variability of electrical coupling. *F*: scatter plot for all the recorded cells in sequential recordings (n = 10 paired recordings) shows no correlation between their synaptic strength (expressed as junctional conductance) and intersomatic distance.

Functional Implications

Although its exact function remains to be elucidated, electrical coupling is believed to play an essential role in olivary function (Llinas et al. 1974; Welsh et al. 1995; De Zeeuw et al. 1998; Placantonakis et al. 2004; Leznik and Llinas 2005; Kistler and DeZeeuw 2005; Blenkinsop and Lang 2006; Placantonakis et al. 2006; Van Der Giessen et al. 2008). For example, clusters of synchronized IO neurons were reported to be dynamically sculpted as a result of transient regulation of electrical coupling by GABAergic inputs originated in the deep cerebellar nuclei (Llinas et al. 1974; Leznik and Llinas 2005). These transiently formed compartments are thought to encode important functional parameters by promoting synchronous "complex spikes" (characteristic burstlike action potentials in climbing fibers) that instruct sets of Purkinje cells in the cerebellar cortex (Leznik and Llinas 2005; Blenkisop and Lang 2006). Our results indicate that the formation of these transient compartments takes place on a network of heterogeneously

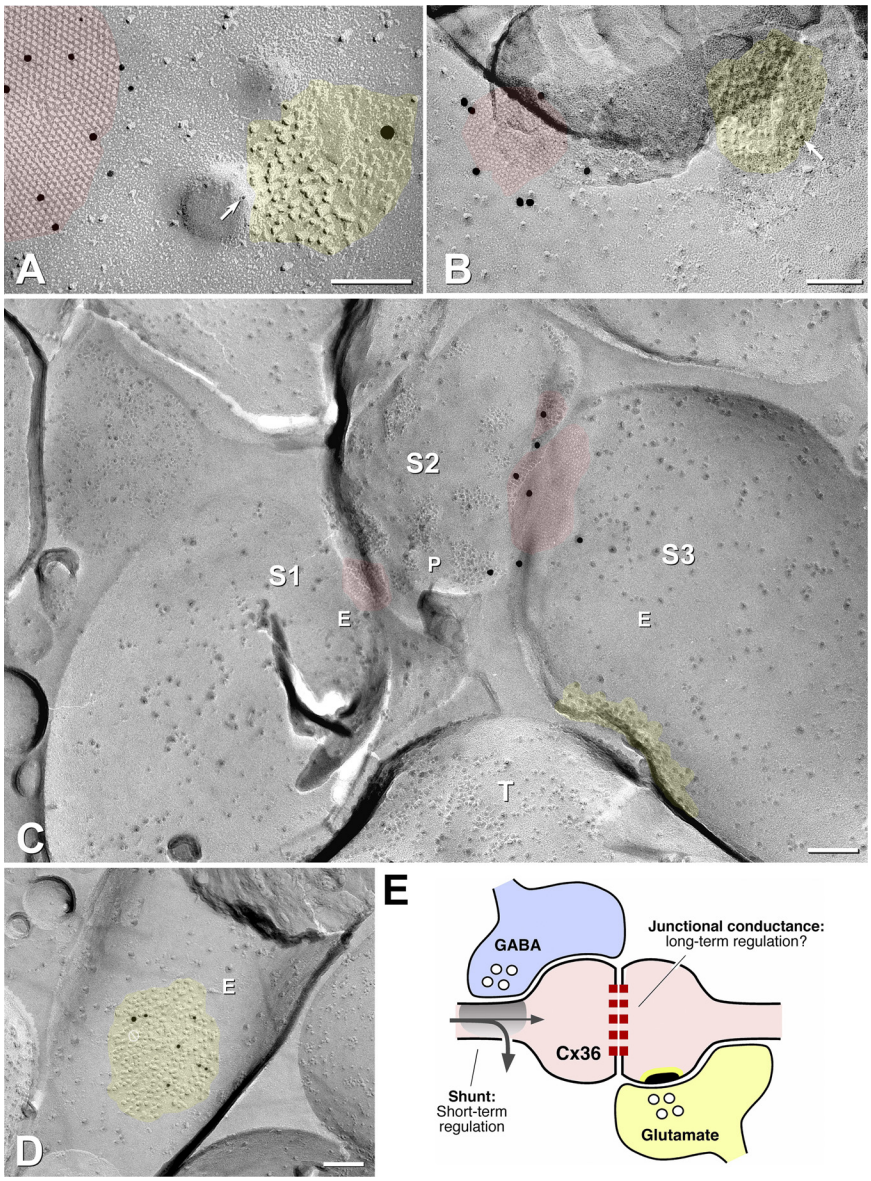

Fig. 8. Close proximity of *N*-methyl-D-aspartate receptor-containing postsynaptic densities (PSDs) to connexin 36 (Cx36)-containing gap junctions in IO glomeruli. *A*: freeze-fracture immunogold labeling (FRIL) shows the presence of Cx35 and NMDA receptors in a single goldfish mixed synapse. Cx35 in a gap junction plaque (pink area) is labeled with 10-nm gold beads. An aggregate of E-face particles (yellow), representing a subsynaptic membrane PSD of a glutamatergic synapse, has one 6-nm (arrow) and one 18-nm gold bead, both independently indicating the presence of NR1 subunits of NMDA receptors. *B*: FRIL double labeling for Cx36 and NR1 in a rat IO neuron. Image shows a double-labeled synapse with NR1 in the PSD labeled by one 10-nm gold bead (arrow) and a gap junction labeled for Cx36 by eight 20-nm gold beads. (One gold bead is hidden behind the vertical fold of a carbon flake lying across the gap junction.) *C*: FRIL image shows the close proximity of an E-face particle aggregate (PSD) in S3 that is postsynaptic to an axon terminal process (T). The PSD is also in close proximity to a gap junction formed between processes S2 and S3. S1–S3 likely correspond to spine processes of IO neurons in this glomerulus within the IO. E and P, membrane E face and P face, respectively. A second gap junction (pink) links processes S2 and S1. There were no immunogold beads at this gap junction, presumably because of relatively low labeling efficiency of this replica (1:100), wherein the 80–100 connexins of this smaller gap junctions would have had a low probability of labeling. Alternatively, absence of labeling could be due to the presence primarily of a connexin other than Cx36 in that small junction (Li et al. 2008). *D*: aggregate of E-face particles (yellow) in an IO neuron, labeled with 10- and 12-nm gold beads, indicating the presence of glutamate NR1 receptor subunits. This labeling confirms that the particles correspond to a glutamatergic postsynaptic density. Calibration bar, 0.1 μm. *E*: does regulation of gap junctional conductance occur in the IO? The tight anatomical arrangement of the glomerulus favors the interaction between chemical and electrical synapses in the IO. GABAergic synapses briefly uncouple IO neurons by shunting the nonjunctional membrane conductance. Our results suggest that, in addition, short-range mechanisms for regulation of gap junction channels by glutamatergic synapses might also occur at IO glomeruli.

coupled IO neurons, where some might not always be coupled. Variations in the degree of coupling might not only finely determine the degree of synchronization between IO neurons within a compartment (see below) but might also determine the ability of individual IO neurons to participate in these coupled compartments.

Electrical coupling is essential for the synchronization of IO neurons that leads to proper timing of their action potentials (Long et al. 2002) and thereby for learning-dependent timing in cerebellar motor control (Van Der Giessen et al. 2008). Analysis of Cx36-deficient mice revealed impaired timing of both locomotion and eye-blink response, together with an increased variability in the latencies of spike activities in response to the unconditioned stimulus (Van Der Giessen et al. 2008). These differences in spike timing were found to result from altered interactions with subthreshold oscillations, likely as a result of the decrease of synchronization between IO neurons in Cx36-deficient animals (Van Der Giessen et al. 2008). Subthreshold oscillations (Llinas and Yarom 1986; Lampl and Yarom 1997) are considered an essential timing mechanism that regulates the output of the downstream Purkinje cells (Welsh et al. 1995; Yarom and Cohen 2002). The heterogeneity of coupling between IO neurons that we report in the present study suggests that climbing fibers might convey more complex information to the cerebellar cortex, because differences in coupling might finely influence synchronization among climbing fibers and in this manner regulate learning-dependent timing in the olivocerebellar network. Supporting this possibility, a recent report challenged the view that the climbing fibers convey an all-or-none signal to the cerebellar cortex (Mathy et al. 2009). That study elegantly demonstrated that the number of spikes in the burst of a complex spike in a climbing fiber depends on the phase of subthreshold oscillations, thereby encoding the state of the olivary network. The bursts of the climbing fibers are transmitted to the cerebellar cortex, where they have a significant impact on Purkinje cells, since they were shown to promote short-term and long-term plasticity at parallel fiber synapses in a manner dependent on the number of spikes contained in the burst (Mathy et al. 2009). Heterogeneity of coupling between IO neurons might finely influence synchro-

nization and properties of climbing fibers and, as a result, their probability of eliciting plastic changes in the cerebellar cortex. If dynamic, heterogeneity of electrical coupling between IO neurons could represent a novel learning mechanism within the olivocerebellar system, where multiple learning mechanisms have been reported (Llinas et al. 1975; Welsh and Harvey 1998; Hansel and Linden 2000; Pugh and Raman 2006; Van Der Giessen et al. 2008; Mathy et al. 2009; for review see Hansel et al. 2001).

The essence of brain function arguably resides on the diversity of its mechanisms for intercellular communication and, perhaps more importantly, on their variability. The remarkable heterogeneity of coupling between IO neurons that we report in this study reveals an unexpected degree of complexity of olivary networks. Interestingly, a recent report has suggested that the existence of coupling heterogeneity is a critical characteristic of the Golgi cell network in the cerebellum, where electrical synapses can underlie desynchronization (Vervaeke et al. 2010; see also Connors et al. 2010). Thus heterogeneity of coupling may represent a general property of networks of extensively coupled neurons and underlie important functions in various mammalian brain structures.

ACKNOWLEDGMENTS

We thank Ramani Balu for early contributions to tracer-coupling studies and Pamela Cabahug for assistance with the confocal microscope. We also thank Sebastian Curti for useful discussions and comments on the manuscript.

GRANTS

This research was supported by National Institutes of Health Grants DC03186 and NS0552827 to A. E. Pereda; S10RR05831 (JEOL 2000 EXII), S10RR08329 (JEOL 9010c), NS044395, and NS044010 to J. E. Rash; and MH081935 to P. E. Castillo.

DISCLOSURES

No conflicts of interest, financial or otherwise, are declared by the author(s).

REFERENCES

Alev C, Urschel S, Sonntag S, Zoidl G, Fort AG, Hoher T, Matsubara M, Willecke K, Spray DC, Dermietzel R. The neuronal connexin36 interacts with and is phosphorylated by CaMKII in a way similar to CaMKII interaction with glutamate receptors. *Proc Natl Acad Sci USA* 105: 20964–20969, 2008.

Bal T, McCormick DA. Synchronized oscillations in the inferior olive are controlled by the hyperpolarization-activated cation current I_h. *J Neurophysiol* 77: 3145–3156, 1997.

Bennett MV. Physiology of electrotonic junctions. *Ann NY Acad Sci* 137: 509–539, 1966.

Bennett MV, Zukin RS. Electrical coupling and neuronal synchronization in the Mammalian brain. *Neuron* 41: 495–511, 2004.

Best AR, Regehr WG. Inhibitory regulation of electrically coupled neurons in the inferior olive is mediated by asynchronous release of GABA. *Neuron* 62: 555–565, 2009.

Blenkinsop TA, Lang EJ. Block of inferior olive gap junctional coupling decreases Purkinje cell complex spike synchrony and rhythmicity. *J Neurosci* 26: 1739–1748, 2006.

Branton D, Bullivant S, Gilula NB, Karnovsky MJ, Moor H, Muhlethaler K, Northcote DH, Packer L, Satir B, Satir P, Speth V, Staehlin LA, Steere RL, Weinstein RS. Freeze-etching nomenclature. *Science* 190: 54–56, 1975.

Condorelli DF, Parenti R, Spinella F, Trovato Salinaro A, Belluardo N, Cardile V, Cicirata F. Cloning of a new gap junction gene (Cx36) highly expressed in mammalian brain neurons. *Eur J Neurosci* 10: 1202–1208, 1998.

Connors BW, Long MA. Electrical synapses in the mammalian brain. *Annu Rev Neurosci* 27: 393–418, 2004.

Connors BW, Zolnik TA, Lee SC. Enhanced functions of electrical junctions. *Neuron* 67: 354–356, 2010.

Cusato K, Bosco A, Rozental R, Guimaraes CA, Reese BE, Linden R, Spray DC. Gap junctions mediate bystander cell death in developing retina. *J Neurosci* 23: 6413–6422, 2003.

De Zeeuw CI, Holstege JC, Ruigrok TJ, Voogd J. Mesodiencephalic and cerebellar terminals terminate upon the same dendritic spines in the glomeruli of the cat and rat inferior olive: an ultrastructural study using a combination of [^{3}H]leucine and wheat germ agglutinin coupled horseradish peroxidase anterograde tracing. *Neuroscience* 34: 645–655, 1990.

De Zeeuw CI, Simpson JI, Hoogenraad CC, Galjart N, Koekkoek SK, Ruigrok TJ. Microcircuitry and function of the inferior olive. *Trends Neurosci* 21: 391–400, 1998.

Dinchuk JE, Johnson TJ, Rash JE. Postreplication labeling of E-leaflet molecules: membrane immunoglobulins localized in sectioned, labeled replicas examined by TEM and HVEM. *J Electron Microsc Tech* 7: 1–16, 1987.

Devor A, Yarom Y. Electrotonic coupling in the inferior olivary nucleus revealed by simultaneous double patch recordings. *J Neurophysiol* 87: 3048–3058, 2002.

Flores CE, Cachope R, Nannapaneni S, Ene S, Nairn AC, Pereda AE. Variability of distribution of Ca^{2+}/calmodulin-dependent kinase II at mixed synapses on the Mauthner cell: colocalization and association with connexin 35. *J Neurosci* 30: 9488–9499, 2010.

Fujimoto K. Freeze-fracture replica electron microscopy combined with SDS digestion for cytochemical labeling of integral membrane proteins. Application to the immunogold labeling of intercellular junctional complexes. *J Cell Sci* 108: 3443–3449, 1995.

Gibson JR, Beierlein M, Connors BW. Two networks of electrically coupled inhibitory neurons in neocortex. *Nature* 402: 75–79, 1999.

Hansel C, Linden DJ. Long-term depression of the cerebellar climbing fiber-Purkinje neuron synapse. *Neuron* 26: 473–482, 2000.

Hansel C, Linden DJ, D'Angelo E. Beyond parallel fiber LTD: the diversity of synaptic and non-synaptic plasticity in the cerebellum. *Nat Neurosci* 4: 467–475, 2001.

Harris KM, Landis DM. Membrane structure at synaptic junctions in area CA1 of the rat hippocampus. *Neuroscience* 19: 857–872, 1986.

Kistler WM, De Zeeuw CI. Gap junctions synchronize synaptic input rather than spike output of olivary neurons. *Prog Brain Res* 148: 189–197, 2005.

Kothmann WW, Massey SC, O'Brien J. Dopamine-stimulated dephosphorylation of connexin 36 mediates AII amacrine cell uncoupling. *J Neurosci* 29: 14903–14911, 2009.

Lampl I, Yarom Y. Subthreshold oscillations and resonant behavior: two manifestations of the same mechanism. *Neuroscience* 78: 325–341, 1997.

Landisman CE, Connors BW. Long-term modulation of electrical synapses in the mammalian thalamus. *Science* 310: 1809–1813, 2005.

Leznik E, Llinas R. Role of gap junctions in synchronized neuronal oscillations in the inferior olive. *J Neurophysiol* 94: 2447–2456, 2005.

Li X, Kamasawa N, Ciolofan C, Olson CO, Lu S, Davidson KG, Yasumura T, Shigemoto R, Rash JE, Nagy JI. Connexin45-containing neuronal gap junctions in rodent retina also contain connexin36 in both apposing hemiplaques, forming bihomotypic gap junctions, with scaffolding contributed by zonula occludens-1. *J Neurosci* 28: 9769–9789, 2008.

Llinas R, Baker R, Sotelo C. Electrotonic coupling between neurons in cat inferior olive. *J Neurophysiol* 37: 560–571, 1974.

Llinas R, Walton K, Hillman DE, Sotelo C. Inferior olive: its role in motor learning. *Science* 190: 1230–1231, 1975.

Llinas R, Yarom Y. Electrophysiology of mammalian inferior olivary neurones in vitro. Different types of voltage-dependent ionic conductances. *J Physiol* 315: 549–567, 1981.

Llinas R, Yarom Y. Oscillatory properties of guinea-pig inferior olivary neurones and their pharmacological modulation: an in vitro study. *J Physiol* 376: 163–182, 1986.

Long MA, Deans MR, Paul DL, Connors BW. Rhythmicity without synchrony in the electrically uncoupled inferior olive. *J Neurosci* 22: 10898–10905, 2002.

Marder E, Goaillard JM. Variability, compensation and homeostasis in neuron and network function. *Nat Rev Neurosci* 7: 563–574, 2006.

Mathy A, Ho SS, Davie JT, Duguid IC, Clark BA, Hausser M. Encoding of oscillations by axonal bursts in inferior olive neurons. *Neuron* 62: 388–399, 2009.

Mills SL, Massey SC. The kinetics of tracer movement through homologous gap junctions in the rabbit retina. *Vis Neurosci* 15: 765–777, 1998.

Pan F, Mills SL, Massey SC. Screening of gap junction antagonists on dye coupling in the rabbit retina. *Vis Neurosci* 24: 609–618, 2007.

Parker PR, Cruikshank SJ, Connors BW. Stability of electrical coupling despite massive developmental changes of intrinsic neuronal physiology. *J Neurosci* 29: 9761–9770, 2009.

Pereda A, O'Brien J, Nagy JI, Bukauskas F, Davidson KG, Kamasawa N, Yasumura T, Rash JE. Connexin35 mediates electrical transmission at mixed synapses on Mauthner cells. *J Neurosci* 23: 7489–7503, 2003a.

Pereda A, O'Brien J, Nagy JI, Smith M, Bukauskas F, Davidson KG, Kamasawa N, Yasumura T, Rash JE. Short-range functional interaction between connexin35 and neighboring chemical synapses. *Cell Commun Adhes* 10: 419–423, 2003b.

Pereda AE, Bell TD, Chang BH, Czernik AJ, Nairn AC, Soderling TR, Faber DS. Ca^{2+}/calmodulin-dependent kinase II mediates simultaneous enhancement of gap-junctional conductance and glutamatergic transmission. *Proc Natl Acad Sci USA* 95: 13272–13277, 1998.

Pereda AE, Faber DS. Activity-dependent short-term enhancement of intercellular coupling. *J Neurosci* 16: 983–992, 1996.

Pereda AE, Rash JE, Nagy JI, Bennett MV. Dynamics of electrical transmission at club endings on the Mauthner cells. *Brain Res Brain Res Rev* 47: 227–244, 2004.

Placantonakis DG, Bukovsky AA, Aicher SA, Kiem HP, Welsh JP. Continuous electrical oscillations emerge from a coupled network: a study of the inferior olive using lentiviral knockdown of connexin36. *J Neurosci* 26: 5008–5016, 2006.

Placantonakis DG, Bukovsky AA, Zeng XH, Kiem HP, Welsh JP. Fundamental role of inferior olive connexin 36 in muscle coherence during tremor. *Proc Natl Acad Sci USA* 101: 7164–7169, 2004.

Pugh JR, Raman IM. Potentiation of mossy fiber EPSCs in the cerebellar nuclei by NMDA receptor activation followed by postinhibitory rebound current. *Neuron* 51: 113–123, 2006.

Rash JE, Duffy HS, Dudek FE, Bilhartz BL, Whalen LR, Yasumura T. Grid-mapped freeze-fracture analysis of gap junctions in gray and white matter of adult rat central nervous system, with evidence for a "panglial syncytium" that is not coupled to neurons. *J Comp Neurol* 388: 265–292, 1997.

Rash JE, Pereda A, Kamasawa N, Furman CS, Yasumura T, Davidson KG, Dudek FE, Olson C, Li X, Nagy JI. High-resolution proteomic mapping in the vertebrate central nervous system: close proximity of connexin35 to NMDA glutamate receptor clusters and co-localization of connexin36 with immunoreactivity for zonula occludens protein-1 (ZO-1). *J Neurocytol* 33: 131–151, 2004.

Rash JE, Staines WA, Yasumura T, Patel D, Furman CS, Stelmack GL, Nagy JI. Immunogold evidence that neuronal gap junctions in adult rat brain and spinal cord contain connexin-36 but not connexin-32 or connexin-43. *Proc Natl Acad Sci USA* 97: 7573–7578, 2000.

Rash JE, Yasumura T. Direct immunogold labeling of connexins and aquaporin-4 in freeze-fracture replicas of liver, brain, and spinal cord: factors limiting quantitative analysis. *Cell Tissue Res* 296: 307–321, 1999.

Rash JE, Yasumura T, Dudek FE. Ultrastructure, histological distribution, and freeze-fracture immunocytochemistry of gap junctions in rat brain and spinal cord. *Cell Biol Int* 22: 731–749, 1998.

Smith M, Pereda AE. Chemical synaptic activity modulates nearby electrical synapses. *Proc Natl Acad Sci USA* 100: 4849–4854, 2003.

Takumi Y, Ramirez-Leon V, Laake P, Rinvik E, Ottersen OP. Different modes of expression of AMPA and NMDA receptors in hippocampal synapses. *Nat Neurosci* 2: 618–624, 1999.

Urbano FJ, Leznik E, Llinas RR. Modafinil enhances thalamocortical activity by increasing neuronal electrotonic coupling. *Proc Natl Acad Sci USA* 104: 12554–12559, 2007.

Urschel S, Hoher T, Schubert T, Alev C, Sohl G, Worsdorfer P, Asahara T, Dermietzel R, Weiler R, Willecke K. Protein kinase A-mediated phosphorylation of connexin36 in mouse retina results in decreased gap junctional communication between AII amacrine cells. *J Biol Chem* 281: 33163–33171, 2006.

Van Der Giessen RS, Koekkoek SK, van Dorp S, De Gruijl JR, Cupido A, Khosrovani S, Dortland B, Wellershaus K, Degen J, Deuchars J, Fuchs EC, Monyer H, Willecke K, De Jeu MT, De Zeeuw CI. Role of olivary electrical coupling in cerebellar motor learning. *Neuron* 58: 599–612, 2008.

Veruki ML, Hartveit E. Meclofenamic acid blocks electrical synapses of retinal AII amacrine and on-cone bipolar cells. *J Neurophysiol* 101: 2339–2347, 2009.

Vervaeke K, Lorincz A, Gleeson P, Farinella M, Nusser Z, Silver RA. Rapid desynchronization of an electrically coupled interneuron network with sparse excitatory synaptic input. *Neuron* 67: 435–451, 2010.

Weber JT, De Zeeuw CI, Linden DJ, Hansel C. Long-term depression of climbing fiber-evoked calcium transients in Purkinje cell dendrites. *Proc Natl Acad Sci USA* 100: 2878–2883, 2003.

Welsh JP, Harvey JA. Acute inactivation of the inferior olive blocks associative learning. *Eur J Neurosci* 10: 3321–3332, 1998.

Welsh JP, Lang EJ, Sugihara I, Llinas R. Dynamic organization of motor control within the olivocerebellar system. *Nature* 374: 453–457, 1995.

Yang XD, Korn H, Faber DS. Long-term potentiation of electrotonic coupling at mixed synapses. *Nature* 348: 542–545, 1990.

Yarom Y, Cohen D. The olivocerebellar system as a generator of temporal patterns. *Ann NY Acad Sci* 978: 122–134, 2002.

Zheng N, Raman IM. Synaptic inhibition, excitation, and plasticity in neurons of the cerebellar nuclei. *Cerebellum* 9: 56–66, 2010.

Zsiros V, Maccaferri G. Noradrenergic modulation of electrical coupling in GABAergic networks of the hippocampus. *J Neurosci* 28: 1804–1815, 2008.